

Complex Formation between Polyelectrolytes and Oppositely Charged Oligoelectrolytes

Jiajia Zhou,^{1,2,*} Matthias Barz,³ and Friederike Schmid^{2,†}

¹*School of Chemistry & Environment, Center of Soft Matter Physics and Its Applications
Beihang University, Xueyuan Road 37, Beijing 100191, China*

²*Komet 331, Institute of Physics, Johannes Gutenberg-University Mainz
Staudingerweg 9, D55099 Mainz, Germany*

³*Institute of Organic Chemistry, Johannes Gutenberg-University Mainz
Duesbergweg 10-14, D55099 Mainz, Germany*

(Dated: August 28, 2021)

We study the complex formation between one long polyanion chain and many short oligocation chains by computer simulations. We employ a coarse-grained bead-spring model for the polyelectrolyte chains, and model explicitly the small salt ions. We systematically vary the concentration and the length of the oligocation, and examine how the oligocations affects the chain conformation, the static structure factor, the radial and axial distribution of various charged species, and the number of bound ions in the complex. At low oligocation concentration, the polyanion has an extended structure. Upon increasing the oligocation concentration, the polyanion chain collapses and forms a compact globule, but the complex still carries a net negative charge. Once the total charge of the oligocations is equal to that of the polyanion, the collapse stops and is replaced by a slow expansion. In this regime, the net charge on the complexes is positive or neutral, depending on the microion concentration in solution. The expansion can be explained by the reduction of the oligocation bridging. We find that the behavior and the structure of the complex are largely independent of the length of oligocations, and very similar to that observed when replacing the oligocations by multivalent salt cations, and conclude that the main driving force keeping the complex together is the release of monovalent counterions and coions. We speculate on the implications of this finding for the problem of controlled oligolyte release and oligolyte substitution.

I. INTRODUCTION

Polyelectrolytes are linear macromolecules composed of ionizable groups [1]. Many important macromolecules in biology are polyelectrolytes, such as DNA and proteins. Polyelectrolytes are usually water soluble and are therefore widely used in water-based organic formulations, which are of great technological interest due to their economical and environmental benefits. When dissolved in water, the ionizable groups dissociate into small mobile ions and leave the chain backbone with the opposite charge. The electrostatic interaction strongly influences the chain conformations. Due to the interplay of short-range excluded volume and long-range electrostatic interactions, and the presence of the small ions, polyelectrolyte solutions display a rich variety of intriguing phenomena, and their behavior is much less understood than that of neutral polymer solutions. Therefore, they are also a rewarding subject for theoretical and simulation studies [2, 3].

Polyelectrolytes can be categorized into weak polyelectrolytes or strong polyelectrolytes, depending on the fraction of charged monomers. In strong polyelectrolytes, the Coulomb repulsion between charged monomers forces the chains to expand, and their resulting radius of gyration is much larger than that of a neutral Gaussian chain of the

same length. Many applications of polyelectrolyte solutions depend on the possible control of the chain conformations. For example, the rheology of a polyelectrolyte solution changes dramatically when the polyelectrolyte conformations change from extended structures to compact globules [4, 5]. The resulting rapid variation in the viscosity of the solution has found many industrial applications, such as the automobile brake system. Another notable example is non-viral gene delivery, where a therapeutic DNA or RNA is transferred into specific cells of patients [6, 7]. The genetic materials are required to pass many obstacles, to penetrate the cell and nuclear membranes. These tasks can only be performed efficiently when the size of the delivery vector is a few tens to several hundreds nanometers. In addition, the morphology of the complex is expected to influence its biological functions [8]. Therefore, the conditions of complex formation will affect the complex properties and finally the transfection efficiency.

Polyelectrolyte complexes are aggregates of polyelectrolyte chains and oppositely charged species. Taking polyanions as an example, one can choose many positively charged complexing agents. The most common choice are multivalent salts. The effect of adding multivalent salt cations to polyanion solutions is well documented in the literature [9]. Upon increasing the multivalent salt concentration, the initially homogeneous polyelectrolyte solution becomes phase separated if the salt concentration is higher than a critical value. This critical value is proportional to the polyelectrolyte concen-

* zhou@uni-mainz.de

† friederike.schmid@uni-mainz.de

tration, and essentially corresponds to the value at which the total charge of added multivalent cations neutralizes the total charge of the polyanions. Above this critical concentration, the solution demixes into a dense and viscous precipitate phase and a dilute solution phase. This phase separation is associated with complex formation between the polyanion and multivalent cations, and the complexes aggregate to form the precipitate phase. Upon further increase of the salt concentration, the precipitate dissolves, and the solution transforms back into a homogeneous phase. The reentrance behavior to the disordered phase can also be associated with the reexpansion of the polyanion chain.

Another popular choice of complexing agent is a polyelectrolyte with opposite charge, especially in the field of non-viral gene delivery system [10, 11]. Polymeric transfection systems have been under rapid development for the last two decades, and *in vivo* applications also start to emerge [12]. Because of the flexibility of the polymer chemistry, polyelectrolytes can be synthesized in linear, branched, and dendritic structures. It is also possible to design them such that they contain not only charged monomers, but also include neutral or hydrophobic blocks that may provide multiple functions. One can tailor the complexing polyelectrolytes to fulfill the specific requirements for efficient delivery, which makes polyelectrolytes a popular choice for gene-delivery vectors.

Despite the advance of experimental techniques, the resolution of single polyelectrolyte complexes remains difficult. Simulation studies can help to understand the organization of the complex in molecular detail, if appropriated models are used. They also provide insight into the underlying physics. For example, it is now well understood that complex formation in strong polyelectrolytes is driven by the gain of translational entropy associated with the release of counterions, rather than by the gain of enthalpy due to the electrostatic interactions [13]. Simulations can also help to explore the parameter space, to save the time and money for trial-and-error experiments. So far, most simulation studies have focused on multivalent cations [14–19], or on the complexation of oppositely charged polyelectrolytes with similar length [13, 20–25].

In this work, we study the complex formation of one long polyelectrolyte chain with many short oppositely charged oligoelectrolytes. We systematically vary the concentration of the short chains and analyze the structure and composition of the complex. We use Langevin simulations to study the complex formation. The remainder of this article is organized as follows: In section II, we briefly introduce the simulation model and describe important parameters of the system. We present the simulation results on the complex structure in section III. Finally, we conclude in section IV with a brief summary.

II. SIMULATION MODEL

We employ a coarse-grained model [26] to simulate the flexible polyelectrolyte chains. Our systems contain two types of polyelectrolyte chains which we will label as A-chain and B-chain for better reference: An A-chain is a negatively charged polyelectrolyte (a polyanion) composed of $N_A = 100$ beads, and a B-chain is a positively charged oligomer (an oligocation) composed of N_B beads (N_B in the range of 2–5). We keep the number of A-chain fixed at $n_A = 1$ in the simulation box, and we vary the number of B-chain n_B . Throughout this work, we will characterize the systems in terms of the monomer concentrations, which are given by

$$\rho_A = N_A/V, \quad \rho_B = n_B N_B/V, \quad (1)$$

where V is the volume of the simulation box. Both A- and B-chains are uniformly charged; each bead carries one charge unit. For each polyelectrolyte, a corresponding number of oppositely charged monovalent ions (i.e., N_A cations and $n_B N_B$ anions) is added to the system to make the whole system charge neutral. We shall refer to the cations as counterions (with respect to the A-chain), and to the anion as coions. In Table I, we list all variables to describe different species in the system.

type	length	charge	molecule number	monomer number
A-chain	N_A	-1	1	N_A
B-chain	N_B	+1	n_B	$n_B N_B$
Counterion (+)	1	+1	N_A	N_A
Coion (-)	1	-1	$n_B N_B$	$n_B N_B$

TABLE I: Table of simulation variables.

Short-range excluded volume interactions between each pair of beads are modeled by the repulsive part of the Lennard-Jones interaction (a Weeks-Chandler-Anderson potential [27]).

$$U_{LJ}(r) = \begin{cases} 4\varepsilon \left[\left(\frac{\sigma}{r}\right)^{12} - \left(\frac{\sigma}{r}\right)^6 + \frac{1}{4} \right] & r < \sqrt[6]{2}\sigma \\ 0 & \text{otherwise} \end{cases} \quad (2)$$

where r is the distance between two beads, and ε and σ characterize the energy and length scales. Here the shift of the potential level is chosen such that the potential is zero at the cutoff.

The beads in the polyelectrolyte chains are connected by harmonic springs. This bonded interaction has the form

$$U_{\text{harm}}(r) = \frac{1}{2}K(r - r_b)^2, \quad (3)$$

where r is the distance between two connected beads, K is the spring constant, and r_b is the equilibrium bond length. The parameters are chosen as $K = 5000 \varepsilon/\sigma^{-2}$ and $r_b = \sigma$. For these choices, the bond length fluctuates

within 10% of the equilibrium bond length [14], and chain crossing is prohibited.

Charged beads also interact with each other *via* electrostatic interaction. For monovalent charged beads, the Coulomb interaction can be written as

$$U_{\text{Coul}} = \frac{e^2}{4\pi\epsilon\epsilon_0 r} = k_B T \frac{\ell_B}{r}. \quad (4)$$

Here ϵ is the dielectric constant of the medium and ϵ_0 is the vacuum permittivity, $k_B T$ is the Boltzmann constant times the temperature. The Bjerrum length characterizes the distance at which the electrostatic potential of a pair of unit charges becomes comparable to the thermal energy, $\ell_B = e^2/4\pi\epsilon\epsilon_0 k_B T$. In this study, we focus on strongly charged polyelectrolytes and choose $\ell_B = 3.0 \sigma$. Electrostatic interactions are calculated using the standard P3M method [28, 29].

We perform Langevin simulations on the complex formation, where water is treated implicitly. The effect of the water is incorporated *via* a viscous environment that provides a coupling to a thermal bath in the equations of motions of the beads, and a dielectric background for the Coulomb interaction. The equation of motion for i -th bead is taken as

$$m \frac{d^2 \mathbf{r}_i}{dt^2} = -\xi \mathbf{v}_i - \nabla_{\mathbf{r}_i} U + \mathbf{f}_i(t), \quad (5)$$

where m and ξ are the monomer mass and friction coefficient, respectively. Equation (5) implies that we neglect hydrodynamic interactions, which is acceptable because we are mostly interested in static equilibrium properties of the system. U is the total potential energy consisting of the Lennard-Jones interaction (2), the harmonic spring interaction (3), and the electrostatic interaction (4). The term $\mathbf{f}_i(t)$ refers to a random force that mimicks the effect of thermal motion due to the surrounding solvents. This noise term satisfies the fluctuation-dissipation theorem

$$\langle f_{\alpha i}(t) \cdot f_{\beta j}(t') \rangle = 2k_B T \xi \delta_{\alpha\beta} \delta_{ij} \delta(t - t'), \quad (6)$$

where $\alpha, \beta = x, y, z$ indicating the components of the random force. We have taken the mass of all beads as unit mass. The temperature of the system is set at $k_B T = 1.0 \epsilon$. The friction coefficient is chosen $\xi = 1.0 \tau^{-1}$, where $\tau = \sigma \sqrt{m/\epsilon}$ is the time unit of the simulation. We have used the velocity-Verlet scheme [30, 31] to integrate Eq. (5), with a time step 0.01τ . All simulations are carried out using the open-source package ESPResSo [32].

We consider cubic simulation boxes with two box sizes: one is 100σ and the other one is 25σ . The corresponding A-monomer concentrations are $10^{-4} \sigma^{-3}$ and $6.4 \times 10^{-3} \sigma^{-3}$, respectively. Compared to the size of a freely-jointed chain of 100 monomers, $R_e \sim 10 \sigma$, the corresponding systems are still in the dilute regime for the A-chain. The main effect of the system size is to regulate the density of counterions and coions, as will be discussed below.

We start the simulation with the A-chain in the center of the box, and randomly distributed B-chains. We then

perform the Langevin dynamics simulation until the system reaches equilibrium. This equilibration process normally takes 2×10^6 time steps. After equilibration, we take a snapshot and record the position of each bead every 2000 steps in the following 2×10^6 time steps. Three runs with independent starting configurations are performed for each parameter setting. These results are used to perform a statistical analysis and compute the physical quantities discussed in the next section.

In some cases, we also perform reference simulations with multivalent salt ions. Here we replace the B-chains composed of N_B monovalent charged beads by single beads carrying N_B unit charges. The comparison between the oligocation case and the multivalent salt case can provide insight into the influence of the chain character of oligocations on the structure of the polyelectrolyte complexes.

III. RESULTS AND DISCUSSIONS

A. Single chain conformation

The size and the shape of a polymer chain in solution can be characterized by several quantities. In this section, we calculate these quantities for the polyanion chain and study their dependence on the B-monomer concentration.

Specifically, we compute the time-average of the following quantities:

1. *The radius of gyration.* We monitor the gyration tensor of the A-chain, defined by

$$\mathbf{S} = \frac{1}{N} \sum_{i=1}^N (\mathbf{r}_i - \mathbf{r}_{\text{com}}) \otimes (\mathbf{r}_i - \mathbf{r}_{\text{com}}), \quad (7)$$

where \mathbf{r}_{com} is the center-of-mass position. The gyration tensor can be written as a symmetric 3×3 matrix, which can be diagonalized by a proper rotation. We denote the diagonal elements of the \mathbf{S} -matrix by λ_1^2 , λ_2^2 , and λ_3^2 , and without loss of generality, we assume $\lambda_1^2 \geq \lambda_2^2 \geq \lambda_3^2$. The radius of gyration is given by

$$R_g = \sqrt{\lambda_1^2 + \lambda_2^2 + \lambda_3^2}. \quad (8)$$

2. *The end-to-end distance.* The end-to-end distance is defined as

$$R_e = |\mathbf{r}_1 - \mathbf{r}_N|, \quad (9)$$

where \mathbf{r}_1 and \mathbf{r}_N is the position of the first and the last beads of A-chain. The ratio R_e^2/R_g^2 gives some information about the shape conformation. This ratio increases from a value of 6 (for a Gaussian chain) to 12 (for a rodlike structure).

3. *The hydrodynamic radius.* The hydrodynamic radius, sometimes also called Stokes radius, characterizes the dynamic properties of the whole chain moving in the solvent. It can be computed from

$$R_h = \left[\frac{1}{N^2} \sum_{i \neq j} \frac{1}{r_{ij}} \right]^{-1}, \quad (10)$$

where r_{ij} is the distance between one pair of beads. The ratio R_h/R_g is also an indication of the chain shape. This ratio attains a value of 1.25 for a self-avoiding chain, and about 2.25 for a stiff rod-like chain [16].

4. *The asphericity.* The gyration tensor calculated before contains more information than the average chain size. Using the diagonalized gyration tensor, we can compute two shape descriptors that characterize how much the chain shape deviates from a sphere or a cylinder. One of them is the asphericity,

$$b = \lambda_1^2 - \frac{1}{2}(\lambda_2^2 + \lambda_3^2), \quad (11)$$

which is a non-negative number. A zero value corresponds to a spherical shape ($\lambda_1^2 = \lambda_2^2 = \lambda_3^2$), while for a rod-like object one has $b \approx \lambda_1^2$ ($\lambda_1^2 \gg \lambda_2^2, \lambda_3^2$).

5. *The acylindricity.* The other shape descriptor is the acylindricity,

$$c = \lambda_2^2 - \lambda_3^2, \quad (12)$$

which is also a non-negative number. A zero value corresponds to a shape with uniaxial symmetry, e.g., ellipsoidal or cylindrical ($\lambda_2^2 = \lambda_3^2$), i.e., the object appears circular when projected on to the plane perpendicular to the λ_1 axis. A large positive value indicates a deviation from the cylindrical shape.

The time-averaged values of above quantities for A-monomer concentration $\rho_A = 10^{-4} \sigma^{-3}$ are shown in Fig. 1 as a function of B-monomer concentration. Three different length of B-chains are considered, $N_B = 2, 4$ and 5. In Fig. 2, representative snapshots of the complex are shown for $N_B = 5$ at different B-monomer concentrations: $\rho_B = 2.5 \times 10^{-5}, 10^{-4}$, and $2.5 \times 10^{-4} \sigma^{-3}$.

We start with discussing the lowest B-chain concentration, which is close to the situation of a free A-chain with only its counterions. Since the A-chain is strongly charged, the polyelectrolyte assumes an extended form. The repulsion between like charges on the chain backbone causes the polyelectrolyte to extend, and the end-to-end distance ($\sim 55 \sigma$) is much larger than that of a freely-jointed chain with the same length ($\sqrt{N_{Ar} b} = 10 \sigma$). Nevertheless, the chain conformation is still far from the rigid-rod limit, which would correspond to an end-to-end distance $N_{Ar} b = 100 \sigma$. This is partially due to the

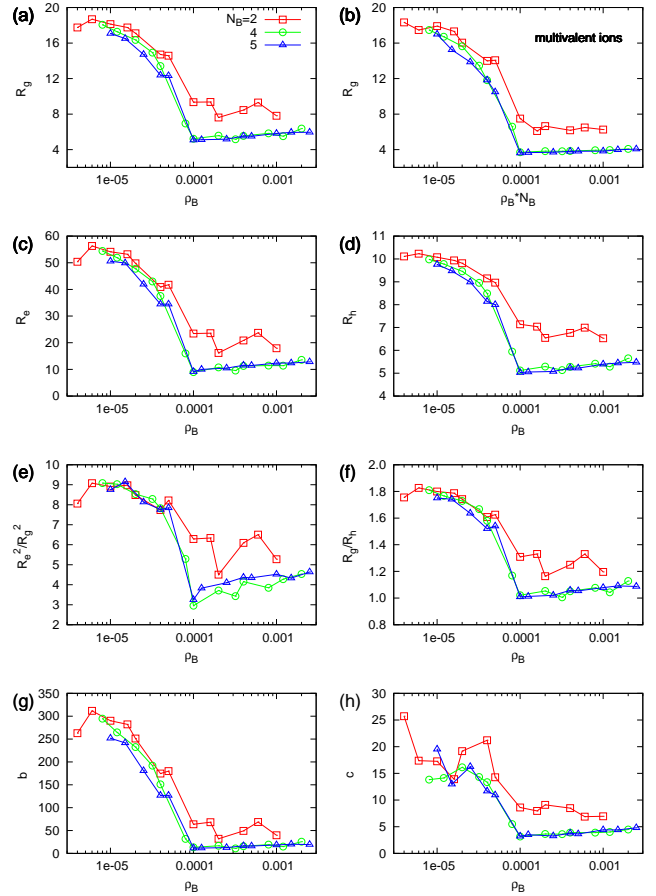


FIG. 1: (a) Radius of gyration R_g , (c) end-to-end distance R_e , (d) hydrodynamic radius R_h , (e) the ratio R_e^2/R_g^2 , (f) the ratio R_h/R_g , (g) the asphericity b , and (h) the acylindricity c , as a function of the B-monomer concentration. The radius of gyration for multivalent salts is shown in (b) for comparison. The A-monomer concentration is $10^{-4} \sigma^{-3}$.

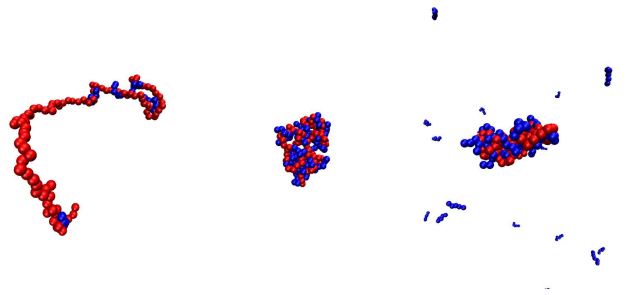


FIG. 2: Snapshots of the polyelectrolyte complex at A-monomer concentration $10^{-4} \sigma^{-3}$. For clarity, only the A-chain (red) and B-chains (blue) are shown. The B-chains have a length of $N_B = 5$, and B-monomer concentrations are $\rho_B = 2.5 \times 10^{-5}, 10^{-4}$, and $2.5 \times 10^{-4} \sigma^{-3}$. Visualization is made by VMD [33].

counterion condensation. In our simulation, the Manning parameter $\Gamma = \ell_B/\ell_Q$, which is the ratio between the Bjerrum length $\ell_B = 3.0\sigma$ and the average charge separation on the polyelectrolyte backbone $\ell_Q = r_b = \sigma$, is equal to 3. When $\Gamma > 1$, most counterions stay close to the polyelectrolyte backbone, effectively reducing the repulsion between the charged beads.

When the B-monomer concentration increases, the behavior of the size of the A-chain reveals two distinct regimes, which are separated by the neutralization concentration $\rho_B = \rho_A = 10^{-4}\sigma^{-3}$. When positive B-chains are added to the solution, two main effects take place. Firstly, the electrostatic attraction between the A- and B-chains causes an accumulation of B-chains around the A-chain backbone. Secondly, the counterions and coions (monovalent cations and anions) are released from the A-chain backbone and from the B-chains into the solution, which is associated with a great gain in entropy. Both effects favor the complex formation, and the latter appears to be the main driving force for the polyelectrolyte complexation in highly charged systems [13]. Once the complex is formed, the A-chain size shows a sharp decrease at small B-monomer concentration. The collapse of the A-chain is driven by the electrostatic interaction. Apart from the fact that it is energetically favorable for the complex to have a compact structure, the B-chains in the complex can also connect two distant monomers on the A-chain backbone, resulting in bridge formation. This is very similar to the ion-bridging effect in multivalent salt solution [34], which we will discuss in Section III E.

The complex reaches its minimum size when the concentration of B-monomer and A-monomer are equal, as all monovalent counterions are replaced by the B-chains. Further increasing the B-chain concentration causes the complex to expand slightly, but the compact globule structure remains. The two ratios [Fig. 1(e) and (f)] and the two shape descriptors [Fig. 1(g) and (h)] display the same features as the radius of gyration. The A-chain initially has an elongated shape, and becomes more spherical as the B-monomer concentration is increased. For longer B-chains $N_B = 4, 5$, the characteristic quantities of the complex are almost independent of the chain length. This indicates that the behavior of the complex is indeed dominated by electrostatics and counterion/coion release, as discussed above, and depends little on the chain characteristics of the oligocations. In contrast, the shortest oligocations ($N_B = 2$) are less effective complexing agents than the longer ones, as evident from the fact that the size of the complex is larger. For such small values of N_B , the translational entropy of the oligomers becomes important and acts against complexation.

For comparison, we also show data for the radius of gyration when the B-chains are replaced by multivalent cations with the same charge [Fig. 1(b)]. The overall trends are similar, and our results are consistent with the simulation studies of Hsiao [17–19]. The size of the complex formed by multivalent cations is slightly smaller

than that of the complex formed by the oligocations, as the overall volume of the multivalent cations is smaller.

The single-chain conformation also depends on the A-monomer concentration. Figure 3 shows the radii and shape descriptors for a higher A-monomer concentration $\rho_A = 6.4 \times 10^{-3}\sigma^{-3}$, and Fig. 4 a selection of representative snapshots. As in the more dilute system (Fig. 1), one observes a chain collapse with increasing ρ_B up to the neutralization point where the B-monomer concentration equals the A-monomer concentration. However, in contrast to Fig. 1, the size of the complex increases significantly when the B-monomer concentration exceeds $\rho_B = \rho_A$. All three radii show a large positive slope as one increases the B-monomer concentration. The change of the chain conformation is also apparent when looking at the snapshots in Fig. 4, which show that the A-chain reexpands at high B-monomer concentration.

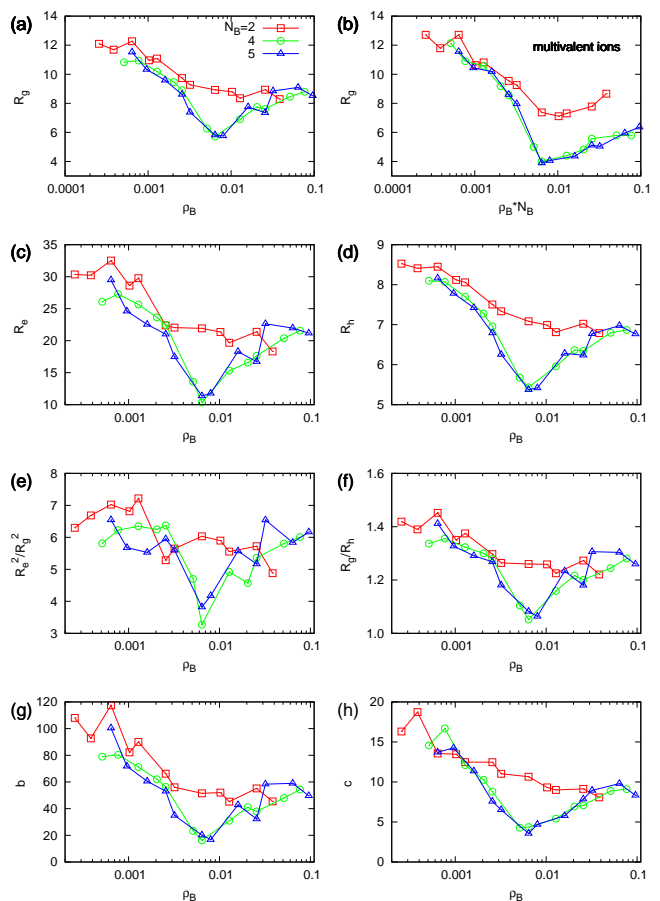


FIG. 3: Similar plots as Fig. 1 for A-monomer concentration $\rho_A = 6.4 \times 10^{-3}\sigma^{-3}$.

This reentrance phenomenon can presumably be explained by the screening effect of the free ions (counterions, coions, and free oligocations), which are much more abundant in this system than in the more dilute system of Fig. 1. Indeed, if one naively extracts a Debye screening length from the microion concentrations

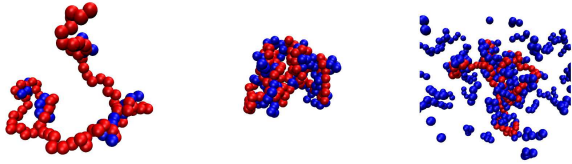


FIG. 4: Snapshots of complexes at A-monomer concentration $6.4 \times 10^{-3} \sigma^{-3}$. For clarity, only the A-chain (red) and B-chains (blue) are shown. The B-chains have a length of $N_B = 4$, and B-monomer concentrations are $\rho_B = 1.6 \times 10^{-3}$, 6.4×10^{-3} , and $1.6 \times 10^{-2} \sigma^{-3}$. Visualization is made by VMD [33].

via $\lambda_D = \sqrt{1/4\pi l_B \sum_c Z_c^2 \rho_c}$ (where the sum c runs over the microion species with valency $Z_c = 1$), one obtains values between $\lambda_D = 16.3 \sigma$ (at $\rho_B \rightarrow 0$), $\lambda_D = 11.5 \sigma$ (at $\rho_B = \rho_A$) up to $\lambda_D = 3.1 \sigma$ (at $\rho_B = 2.5 \times 10^{-3} \sigma^{-3}$) for the dilute systems considered in Fig. 1, hence the Debye screening length always exceeds the Bjerrum length, $\lambda_D > \ell_B$. In the more concentrated system considered in Fig. 3, the screening length ranges between $\lambda_D = 2.0 \sigma$ (at $\rho_B \rightarrow 0$), $\lambda_D = 1.4 \sigma$ (at $\rho_B = \rho_A$) up to $\lambda_D = 1.1 \sigma$ (at $\rho_B = 1.6 \times 10^{-2} \sigma^{-3}$), which is smaller than the Bjerrum length. Here, screening clearly becomes important. This is already apparent from the fact that the characteristic chain radii of bare A-chains (at $\rho_B \rightarrow 0$) are significantly smaller in the concentrated case than in the dilute case, *i.e.*, the electrostatically driven chain stretching is much less pronounced. Upon adding B-chains, the A-chain collapses both in the dilute and in the concentrated system. However, both factors driving the complex formation, the direct electrostatic force between charges as well as the entropy gain associated with counterion/coion release, are reduced at high microion concentrations. Hence the oligocations are less tightly bound to the complex. Beyond the neutralization point, they can more easily change place with excess oligocations in solution; they can move in and out, the complex becomes looser and reexpands. It is interesting to note that right at the neutralization point, the radii and shape factors of the complex are almost the same for the dilute and more concentrated system.

In other respect, the behavior of the A-chain in the more concentrated system is similar to that of the dilute system. As long as the B-chains are not too short, the curves for size and shape parameters versus B-monomer concentration almost lie on top of each other for different chain lengths $N_B = 4, 5$. For short B-chains ($N_B = 2$), the minimum of the radii disappears, and is replaced by a plateau when ρ_B reaches the neutralization concentration. The reference simulations with multivalent ions show that the effect of oligocations is very similar to that of multivalent ions with the same charge.

B. Single-chain structure factor

In this section, we compute the static structure factor of the polyanion chain. This quantity can be measured in scattering experiments and provides essential information about the chain scaling factor. The static structure factor is defined as

$$S(\mathbf{q}) = \frac{1}{N} \sum_{i,j} e^{i\mathbf{q} \cdot (\mathbf{r}_i - \mathbf{r}_j)} \quad (13)$$

where \mathbf{q} is the scattering wavevector. If spherical symmetry can be assumed, the orientation of the wavevector can be integrated out and the structure factor only depends on the magnitude of the wavevector. In Fig. 5, $S(q)$ is plotted for $N_B = 5$ and different ρ_B values. For clarity, the different curves in the figure have been shifted upwards on the y-axis with respect to each other.

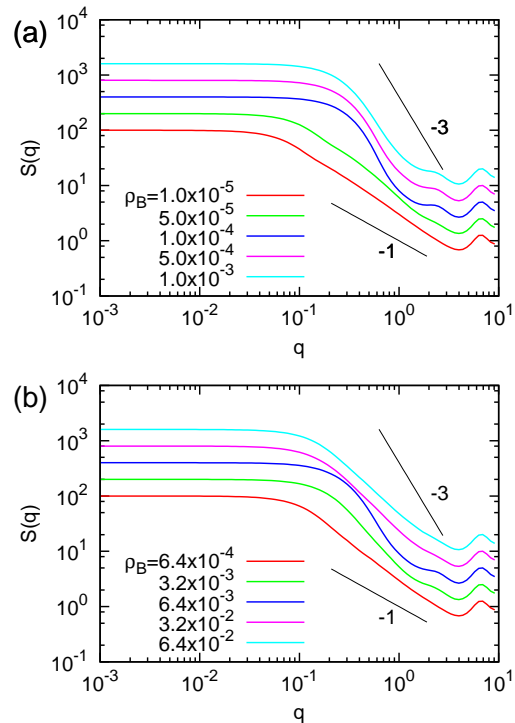


FIG. 5: Static structure factor $S(q)$ of the A-chain for A-monomer concentration (a) $10^{-4} \sigma^{-3}$ and (b) $6.4 \times 10^{-3} \sigma^{-3}$. The B-chains has a length $N_B = 5$. For clarity, the n th curve in each graph has been shifted upwards by multiplying $S(q)$ with a factor 2^{n-1} .

The single-chain structure factor reveals useful information about the characteristic length scales of the polyelectrolyte chain. In our case, there are at least two length scales: one is the radius of gyration R_g , and the other one is the monomer size r_b . In the small wavevector limit, $qR_g \ll 1$, $S(q)$ has a form $N(1 - (qR_g)^2/3)$. In the regime $qr_b > 1$, the self-scattering of the monomer is the only contribution, and $S(q)$ has a universal value of

one. In the intermediate regime ($R_g^{-1} \ll q \ll r_b^{-1}$), $S(q)$ shows power-law behavior. When plotted in a log-log plot, $S(q)$ has a linear slope in this intermediate regime. The slope s can be related to the scaling exponent ν via the relation $\nu = -1/s$. For rodlike chain, one has $\nu = 1$ and $s = -1$, for Gaussian chains, $\nu = 1/2$ and $s = -2$, and for close-packed globules, $\nu = 1/3$ and $s = -3$.

In the dilute systems with A-monomer concentration $10^{-4} \sigma^{-3}$ [Fig. 5(a)], the value of the linear slope starts close to $s = -1$, and changes to a value close to $s = -3$ when the B-monomer concentration increases. The change of the scaling factor indicates that the chain conformation changes from an extended shape to a compact globule structure. At high B-monomer concentrations, a small hump appears in $S(q)$ at around $q = 2$. This indicates that the A-chain is not homogeneously distributed inside the globule. The presence of B-chains induces a certain degree of organization in the A-monomer distribution. In the more concentrated systems with A-monomer density $6.4 \times 10^{-3} \sigma^{-3}$ [Fig. 5(b)], the slope takes the value near $s = -1$, changes to $s = -3$ at intermediate B-monomer concentration, and reverses back to $s = -1$ when the B-chain concentration is high.

We compute the swelling factor ν by performing linear fits to the log-log plots of $S(q)$ in the power-law regime. Figure 6 shows the resulting values for ν as a function of B-monomer concentration for different B-chain lengths. The behavior of the scaling factor is similar to that of the radius of gyration, and the physical picture is similar to what we have described in the last section. For low A-monomer concentration, the scaling factor decreases as the B-chain concentration increases, and reaches a plateau once the neutralization condition is satisfied. For high A-monomer concentration, after the neutralization, the scaling factor starts to increase, indicating a reexpansion of the A-chain.

C. Radial distribution function

The complex not only contains the A-chain, but also the oppositely charged B-chains as well as possibly some counterions and coions. Therefore, it is important to understand how the different species are distributed inside and around the complex. We first follow the standard practice to compute the radial distribution functions. If we choose a type I bead as the center, the radial distribution function $G_{IJ}(r)$ represents the number density of type J beads as a function of the distance r to the central I bead. We have calculated the radial distribution function for A-monomers $G_{AA}(r)$, between one pair of A-monomer and B-monomer $G_{AB}(r)$, and between one pair of A-monomer and counterions $G_{A+}(r)$. These distribution functions are plotted in Fig. 7 for the concentration $\rho_A = \rho_B = 6.4 \times 10^{-3} \sigma^{-3}$. The results for different B-chain length are also shown. For different concentrations, the figures are similar.

The radial distribution functions exhibit relatively lit-

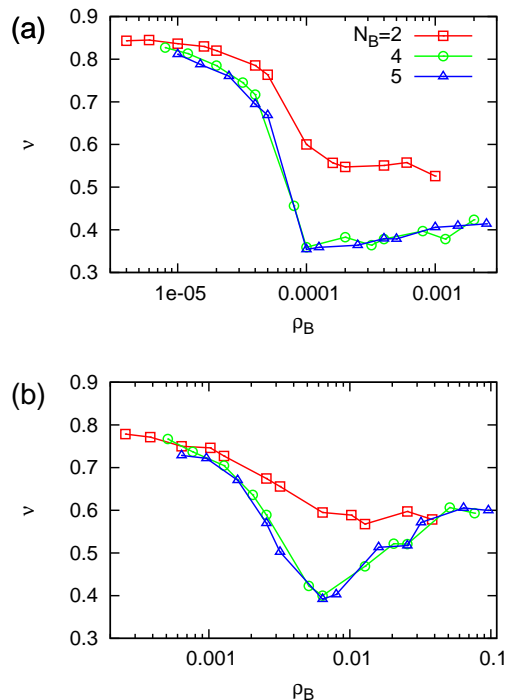


FIG. 6: The scaling factor ν as a function of B-monomer density ρ_B for A-monomer density (a) $10^{-4} \sigma^{-3}$ and (b) $6.4 \times 10^{-3} \sigma^{-3}$.

tle structure, as is characteristic of a fluid. In Fig. 7(a), the first peak at $r = 1 \sigma$ indicates the chain connectivity as the equilibrium bond length is around unit length. There is also a weak second peak around $r = 2 \sigma$, but the correlation smears out at a larger distance, as our polyelectrolyte chain is flexible. Figure 7(b) shows that there is a significant amount of B-monomers in the vicinity of the A-chain. The first peak at $r = 1 \sigma$ gives the closest distance between oppositely charged A- and B-monomers. A relatively weak second peak indicates a loose ordering of the second shell. The peaks in the radial distribution functions get larger when B-chain becomes longer. However, consistent with the findings discussed above in Sec. III A, Fig. 7(a) and (b) demonstrates that the dependence on the B-chain length is very weak for longer chains $N_B = 4, 5$. A small amount of counterions accumulates around the A-monomers for B-chain length $N_B = 2$, which can be seen from the small peaks in Fig. 7(c). The peak value reduces when the B-chains become longer. We note the scale difference between Fig 7(b) and (c), indicating that the B-monomers have a much larger tendency to accumulate around the A-chain than the monovalent counterions.

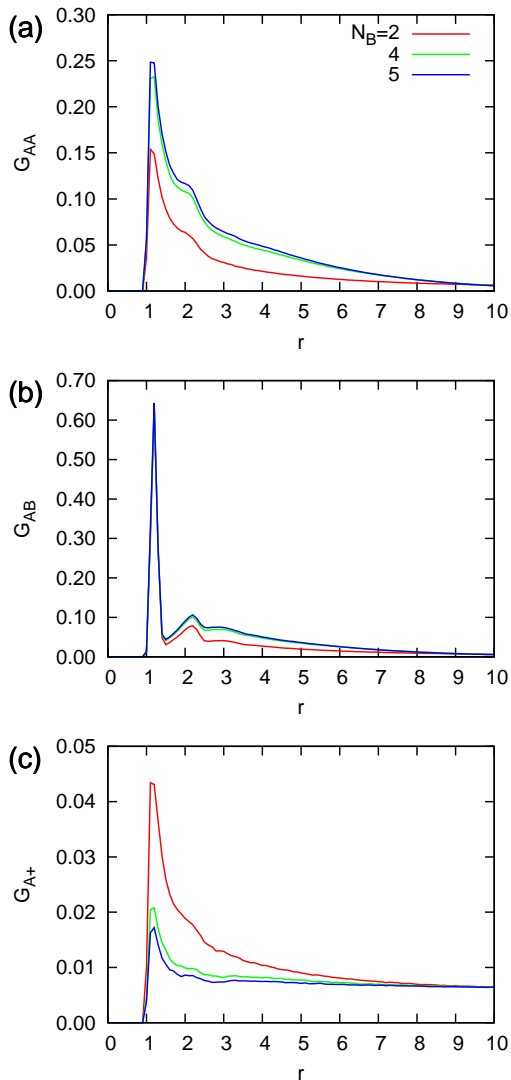


FIG. 7: Representative radial distribution function (a) of A-monomers $G_{AA}(r)$, (b) between A-monomers and B-monomers $G_{AB}(r)$, and (c) between A-monomers and counterions $G_{A+}(r)$. The plots are shown for equal A-monomer and B-monomer concentration, $\rho_A = \rho_B = 6.4 \times 10^{-3} \sigma^{-3}$.

D. Effective charge

Polyelectrolyte chains have a natural direction along the chain, hence it is also instructive to analyze the charge distribution with respect to the polyelectrolyte backbone. Since we consider a flexible polyelectrolyte in the current study, the backbone of the A-chain is not rigid. To determine the charge distribution perpendicular to the backbone, we adopt a method proposed in Refs. [14, 15]: We construct tubes with different radii r around the A-chain backbone. For flexible chains, these tubes do not have a cylinder shape but are more like worm-like tubes. In each snapshot from the simulation,

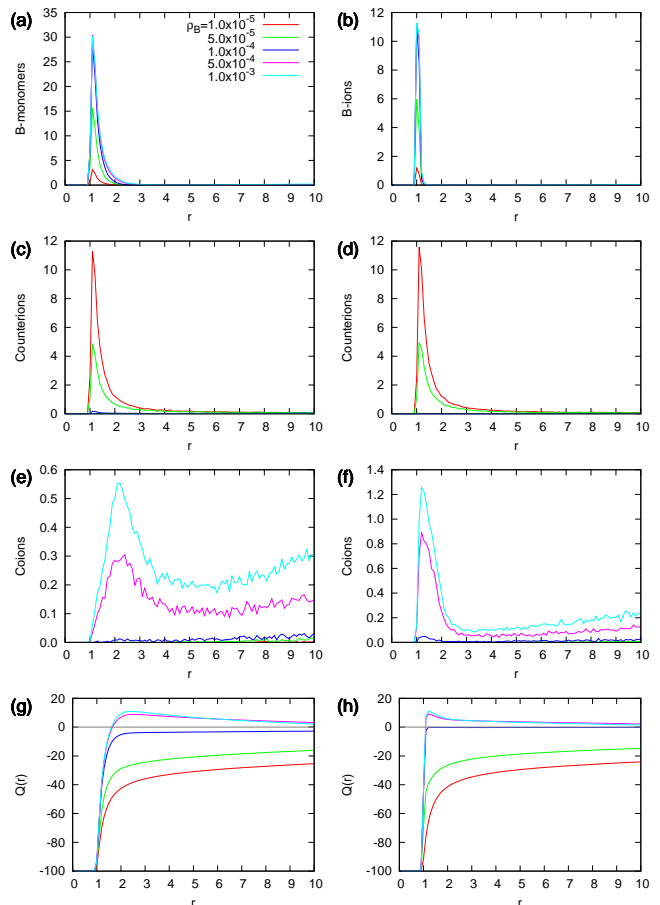


FIG. 8: Axial distribution functions of (a) B-monomers, (c) counterions, and (e) coions. The integrated charge distribution is shown in (g). Here the A-monomer concentration is $10^{-4} \sigma^{-3}$ and the B-chain length $N_B = 5$. The four plots on the left show the oligocation case, and the right (b,d,f,g) the corresponding results for multivalent salt cations.

we count the numbers of various beads between the tubes with radii r and $r + \Delta r$. In this study, we choose a bin size of 0.1σ . Without further normalization, we call this quantity the axial distribution function. One should note that this tube picture is probably not appropriate when the complex takes a globule structure, but the axial quantity still provides some information about how charges are distributed in the direction perpendicular to the backbone. We show the axial distribution functions in Fig. 8 for A-monomer concentration $10^{-4} \sigma^{-3}$ and B-chain length $N_B = 5$. For comparison, we also show the same function for the corresponding system containing multivalent salt cations.

The axial distribution functions show similar features than the radial distribution functions. For B-monomers and counterions, they feature a strong peak at $r = 1 \sigma$. The peak heights depend on the B-monomer concentration: for B-monomers [Fig. 8(a)], the peak height in-

creases as the B-monomer concentration increases, while for counterions [Fig. 8(c)], it decreases. This opposite trend indicates that the highly charged B-chains start to replace the monovalent counterions in the vicinity of the A-chain backbone as the number of B-chains in solution increases. Comparing the structure of complexes containing B-chains with those containing multivalent salt cations, the most pronounced difference is observed for the axial distribution of the negative coions. In the complexes containing multivalent salt cations, the anion peak is more pronounced, while for the case of oligocations, the extension of the coion cloud is broader.

From the axial distribution functions for various charges, we can compute the integrated charge distribution $Q(r)$, which is defined as the total charge of particles inside the tube of radius r . The results are shown in Fig. 8 (g) and (h). The limiting behavior for small r and large $r \rightarrow \infty$ is similar for all B-monomer concentrations. At very short distances, $Q(r)$ is equal to -100 , which is the bare charge of the A-chain. At large distances, $Q(r)$ approaches zero simply due to the electric neutrality condition. The behavior at intermediate distances depends on the concentration of B-chains. Below the neutralization concentration ($\rho_B < \rho_A = 1.0^{-4} \sigma^{-3}$), $Q(r)$ increases monotonically. The value of $Q(r)$ rises sharply at first, then slowly increases to its asymptotic value. For B-monomer concentrations above the neutralization concentration ($\rho_B > \rho_A = 1.0^{-4} \sigma^{-3}$), $Q(r)$ develops a hump at around $r = 2\sigma$. In this case, the positively charged particles bound in the complex overcompensate the bare negative charge of the A-chain already at small distances $r > 1.5\sigma$. The systems containing multivalent salt cations show a similar behavior, except that the hump appears close to $r = 1\sigma$.

These general features do not change significantly as the A-monomer concentration is increased. Fig. 9 shows the axial distribution functions for the systems with A-monomer concentration concentration $6.4 \times 10^{-3} \sigma^{-3}$. Compared to the dilute systems, the main difference is that $Q(r)$ reaches zero much more rapidly, and that it shows a weakly oscillatory behavior at B-chain concentrations above the neutralization concentration. An oscillatory behavior of $Q(r)$ was also observed by Hsiao in simulations of polyelectrolyte complexation with concentrated tetravalent salt ions [19]. Hsiao found that the period of the oscillation matches with the size of the tetravalent ions, suggesting that they can be related to layering. This is consistent with our simulations, where the peak of $Q(r)$ is also broader in the systems containing the (larger) oligocations than in the systems containing multivalent salt cations. Hsiao also found that the structure of $Q(r)$ is more pronounced for tetravalent ions with larger radii. Here, we observe the opposite effect: Even though the size of the oligocations is larger than that of multivalent salt cations, the peak of $Q(r)$ is smaller. This can be attributed to the flexibility of the oligocations, and to the fact that their charge is distributed over several beads.

One may be tempted to determine an effective charge

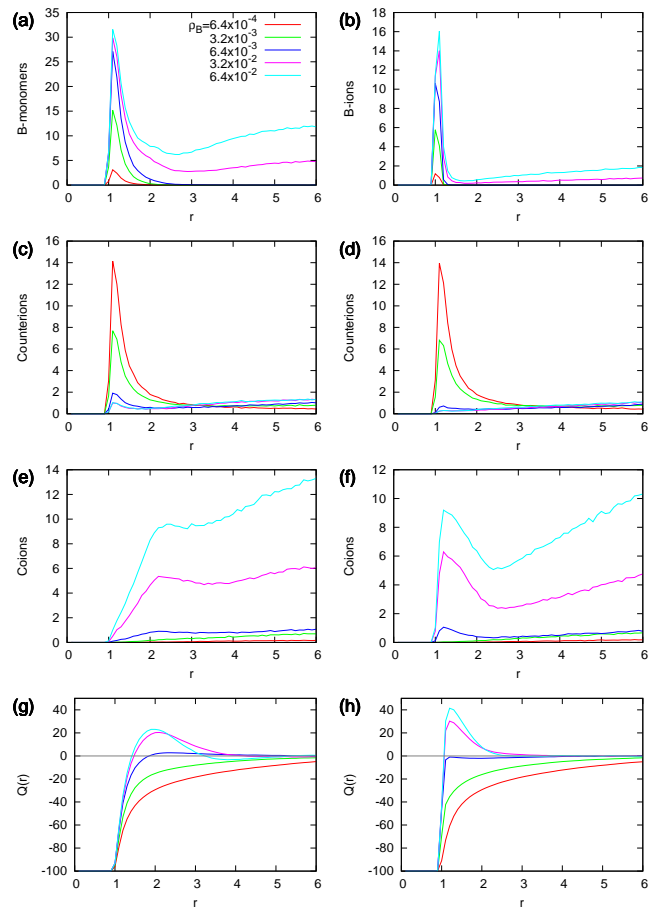


FIG. 9: Same as Fig. 8 for A-monomer concentration $6.4 \times 10^{-3} \sigma^{-3}$.

for the complex as the value of the integrated charge at some cutoff distance r_c , $Q_{\text{eff}} = Q(r_c)$. Important physical quantities such as the electrophoretic mobility of the complex depend on an effective charge. Unfortunately, looking at the data in Fig. 8 (g) and (h), the appropriate choice for the cutoff is not obvious. This becomes even more critical at higher concentrations when the $Q(r)$ oscillates around zero. In such cases, even determining the sign of the effective charge becomes difficult.

Nevertheless, it seems reasonable to define the charge inside the complex by choosing a cutoff in the range of the gyration radius R_g . Here, the situation is relatively clear, and the results do not depend sensitively on the specific choice of the cutoff. At B-monomer (or multivalent salt cation) concentrations below the neutralization condition, the charges on the A-chain are not yet compensated within the distance R_g , hence the complex carries a negative charge. Above the neutralization point, the charge of the complex depends on the A-monomer concentration. In the dilute case [Fig. 8 (g) and (h)], the charges on the oligocations (or multivalent salt cations) enclosed inside the complex exceed the charge of the A-chain, and the complex is positive. In the more con-

centrated case [Fig. 9 (g) and (h)], the charges roughly balance each other and the complex is neutral. Hence complexes exposed to a solution with an excess of oligocations (or multivalent salt cations) tend to fully compensate or even overcompensate the charge on the core A-chain, whereas the compensation is incomplete in a solution which is undersaturated with oligocations or multivalent salt cations.

E. Bound ions

Whereas assigning an effective charge to the polyelectrolyte complex is a somewhat delicate issue, as discussed in the previous section, determining the number of tightly bound ions is much less problematic. We define a charged bead to be bound to the A-chain if its closest distance to the A-chain backbone is less than $r_c = 1.5 \sigma$. Similarly, a B-chain will be called bound if at least one monomer is inside the cutoff distance. Figures 10 and 11 show the average number of bound B-chains, counterions, and coions in the complexes, for $\rho_A = 10^{-4} \sigma^{-3}$ and $6.4 \times 10^{-3} \sigma^{-3}$, respectively. For comparison, the results for multivalent cations are also shown in the right panels [Figs. 10 and 11 (b,d,f, and h)].

The number of bound B-chains increases with the B-monomer concentration. The increase starts gently, but becomes more rapid when the B-monomer concentration approaches the neutralization point. Beyond the neutralization, the number saturates around a fixed value for the dilute case of $\rho_A = 10^{-4} \sigma^{-3}$ [Fig. 10(a)]. The fixed value is determined by the number of B-chains which is necessary to fully compensate the negative charge of the A-chain. In the more concentrated system with $\rho_A = 6.4 \times 10^{-3} \sigma^{-3}$, the number of bound B-chains continues to increase even beyond the neutralization point.

In contrast, the number of bound counterions decreases with the B-monomer concentration. The opposite behavior for counterions and B-chains can be explained by the release of monovalent counterions upon complexation, which is favorable due to the gain in translational entropy. Once the neutralization condition is reached, only very few counterions remain in close vicinity of the A-chain backbone; most of them have been replaced by the B-chain. Coions only appear close to A-chain at high B-monomer concentrations. Their number increases as the B-monomer concentration increases.

Finally, we examine the number of “bridging” oligocations. For multivalent salt cations, de la Cruz *et al.* [34] have argued that the collapse of the strong polyelectrolyte chain is due to ion-bridging, *i.e.*, due to the presence of multivalent cation that connect two distant monomers along the polyanion backbone. At high salt concentration, the ion-bridging is screened by the salt, resulting in a reexpansion of the polyanion chain. A similar argument has been used to explain the coil-globule-coil transition of a polymer chain in mixed cosolvents [35]. In the simulation, we count the number of oligoca-

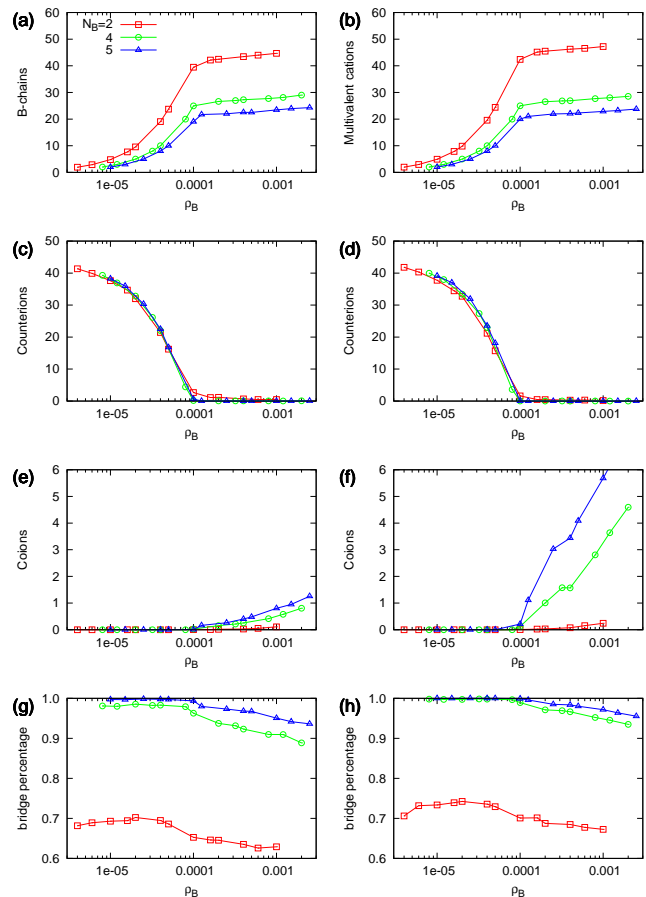


FIG. 10: Number of (a) B-chains, (c) counterions, and (e) coions bound to the A-chain in systems with A-monomer concentration $10^{-4} \sigma^{-3}$. The graphs in the last row show the percentage of the bridges (see the main text). The four graphs on the left show the results for the oligocations case, those on the right the results for multivalent salt cations.

tions that are within cutoff distance of two non-neighbor A-monomers. The ratio between the bridging oligocations and the total number of bound oligocations is plotted in Fig. 10(g) and Fig. 11(g). For longer B-chains ($N_B = 4, 5$), all condensed B-chains participate in bridge formation below the neutralization concentration. When the B-monomer concentration exceeds the neutralization concentration, the bridge ratio is reduced. In the dilute systems with $\rho_A = 10^{-4} \sigma^{-3}$, the reduction is mild [Fig. 10(g)], and this correlates to the small increase of the A-chain size. In the more concentrated system with $\rho_A = 6.4 \times 10^{-3} \sigma^{-3}$, the reduction is significant, and the A-chain reexpands upon increasing B-monomer concentration. A similar behavior is observed for the case of multivalent cations.

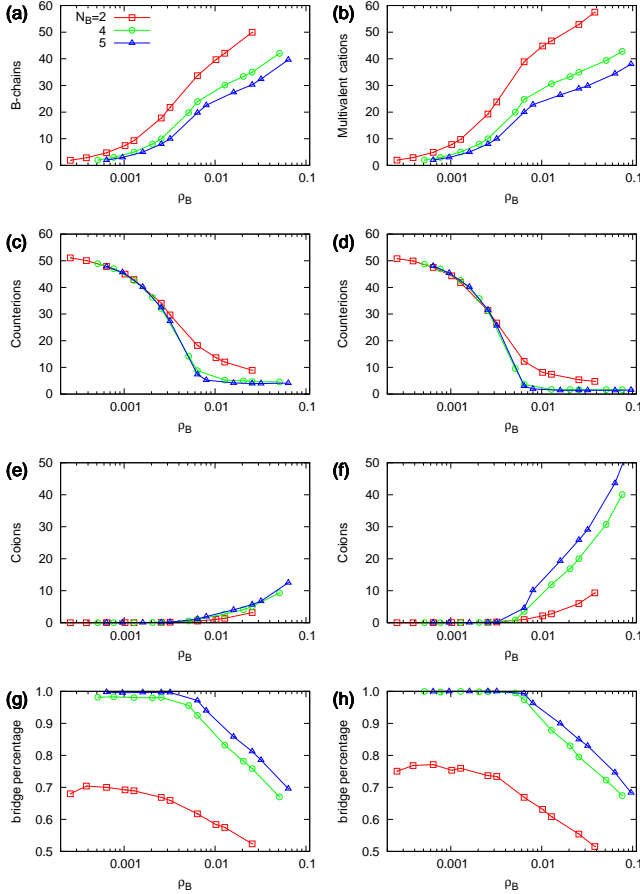


FIG. 11: Same as Fig. 10 for A-monomer concentration $6.4 \times 10^{-3} \sigma^{-3}$.

IV. SUMMARY

In this article, we have studied the complex formation of a flexible polyanion and many short oligocations by Langevin simulations. We employ a coarse-grained bead-spring model for the polyelectrolyte chains, and simulate the small salt ions explicitly. We consider two different polyanion concentrations, and systematically vary the oligocation concentration. We carefully examine how the oligocations affect the chain conformation, the static structure factor, the radial and axial distribution of various charged species, and the amount of ions bound to the polyanion backbone. We also vary the oligocation length and investigate the influences on the complex properties.

The long polyanion chain changes its conformation when the shorter oligocations are added to the solution. Two regimes are observed, which are separated by the neutralization point where the total charge of the oligocations in the system exactly matches the charge on the polyanion. Below the neutralization concentration, the polyanion chain rapidly collapses into to close-packed globule structure as oligocations are added to the system. In this regime, the total charge enclosed

in the globule is still negative, *i.e.*, the bound counterions and oligocations do not fully compensate the charge on the polyanion chain. The behavior in the second regime above the neutralization point depends on the microion concentration. For low microion concentration (if the Debye screening length is much larger than Bjerrum length), the globule stays compact, but the sign of the enclosed charge changes and becomes positive. For higher microion concentration (Debye length smaller than the Bjerrum length), the globule reexpands with increasing oligocation concentration and its net charge almost vanishes. The reexpansion of the polyanion chain can be correlated with a reduction of the fraction of oligocations that bridge between different chain parts.

One particularly noteworthy result of the present study is that the behavior of the complexes of polyelectrolytes with oppositely charged oligolytes is very similar to that of polyelectrolytes with oppositely charged multivalent salt ions. Even more strikingly, it is almost independent of the length of the oligolytes, as long as they are not too short. It only depends on the total concentration of opposite charges on oligolytes or multivalent ions in the solution, compared to the total concentration of polyelectrolyte charge in the solution. Our simulations thus strongly support the idea that the main factor driving the complexation and determining the compactness and structure of the globule is the release of monovalent counterions and coions. The architecture of the multivalent ions seems to be of secondary importance.

If this is correct, it has interesting consequences. In practical applications, one often not only needs to know how to bind molecules within a complex, but also how to release them again. If the dominant force that keeps the complex together is counterion/coion release, then the relative binding strength of oligolytes in the complex solely depends on the oligolyte charge: Oligocations with higher charges will tend to drive out oligocations with smaller charges from the complex for entropic reasons – since a smaller number of highly charged oligocations is necessary to establish the correct charge distribution. Peng and Muthukumar [36] have recently studied how a longer polyelectrolyte chain can substitute a shorter chain in a complex made of oppositely charged polyelectrolyte chains of comparable length. In their case, the substitution is driven by additional counterion release during the process. Based on our results, we predict that it should be possible to induce a similar substitution for complexing oligolytes, which is however driven by the translational entropy of the oligolytes – the counterion/coion entropy does not change during the process.

To quote one technologically relevant example, polyelectrolyte complexes are discussed as potential carriers for siRNA delivery [37]. siRNA molecules (small interfering ribonuclease) are very short pieces of double stranded RNA (about 20-25 nucleotides) which have enormous therapeutic potential [38, 39]. In complexes such as discussed in the present paper, they would take the role of the oligolytes (in this case negatively charged). Once the

carrier has reached its final destination, they could be released most efficiently – according to our results – by exposing the complex to oligolytes that carry a higher charge than the siRNA. The release process is facilitated by the higher concentration of proteins in the cell cytosol. Of course, other factors such as the stiffness of the siRNA may play a role that have not been considered in the present study.

The present simulations were carried out in salt-free conditions, i.e., all microions in the solution were counterions or coions of the polyelectrolyte and oligolytes in the system. Real systems contain salt ions as well. However, the main effect of adding salt is to increase the microion concentration and hence the Debye screening length. We have studied the effect of microion concentration by changing the size of the simulation box, hence we can also use our results to discuss the influence of salt on the behavior of the systems. As discussed above, increasing the microion concentration does not prevent the complex formation, but it does affect the properties of the complex at oligolyte concentrations above the neutralization point: The complex becomes charge neutral, it reexpands upon adding more oligolyte, and the fraction of bridging oligolytes is reduced.

In the present study, we have considered systems containing one long polyelectrolyte, and only varied the number of oligocations in the simulation box. Therefore, we have imposed the constraint that the complex contains only one long polyanion chain, thus focusing on the situation where the polyelectrolyte concentration is very dilute. In reality, complexes may contain several A-chains, and one expects a distribution of complexes with different A-chain numbers. To account for this, it is important not only to understand the structure of one single complex, but also the interaction between different complexes. Furthermore, we have only considered flexible polyelectrolyte chain, whereas most polyelectrolytes are semiflexible. Future studies that include the chain rigidity would be interesting.

ACKNOWLEDGMENTS

This work was funded by the Deutsche Forschungsgemeinschaft (DFG) through the SFB 1066 (project Q1 and A6), and the National Natural Science Foundation of China (NSFC) through the Grant No. 21504004. Computational resources at JGU Mainz (MOGON high performance center) are gratefully acknowledged.

-
- [1] F. Oosawa, *Polyelectrolytes* (Marcel Dekker, New York, 1971).
- [2] J.-L. Barrat and J.-F. Joanny, “Theory of polyelectrolyte solutions,” *Adv. Chem. Phys.* **94**, 1 (1996).
- [3] A. V. Dobrynin and M. Rubinstein, “Theory of polyelectrolytes in solutions and at surfaces,” *Prog. Polym. Sci.* **30**, 1049 (2005).
- [4] R. M. Fuoss, “Polyelectrolytes,” *Discuss. Faraday Soc.* **11**, 125 (1951).
- [5] A. V. Dobrynin, R. H. Colby, and M. Rubinstein, “Scaling theory of polyelectrolyte solutions,” *Macromolecules* **28**, 1859 (1995).
- [6] D. W. Pack, A. S. Hoffman, S. Sun, and P. S. Stayton, “Design and development of polymers for gene delivery,” *Nat. Rev. Drug Discovery* **4**, 581 (2005).
- [7] D. J. Glover, H. J. Lipps, and D. A. Jans, “Towards safe, non-viral therapeutic gene expression in humans,” *Nat. Rev. Genet.* **6**, 299 (2005).
- [8] Kotaro Hayashi, Hiroyuki Chaya, Shigeto Fukushima, Sumiyo Watanabe, Hiroyasu Takemoto, Kensuke Osada, Nobuhiro Nishiyama, Kanjiro Miyata, and Kazunori Kataoka, “Influence of RNA strand rigidity on polyion complex formation with block cationomers,” *Macromol. Rapid Commun.* **37**, 486 (2016).
- [9] V. A. Bloomfield, “DNA condensation by multivalent cations,” *Biopolymers* **44**, 269 (1997).
- [10] E. Wagner, M. Zenke, M. Cotten, H. Beug, and M.L. Birnstiel, “Transferrin-polycation conjugates as carriers for DNA uptake into cells,” *PNAS* **87**, 3410 (1990).
- [11] K. Miyata, N. Nishiyama, and K. Kataoka, “Rational design of smart supramolecular assemblies for gene delivery: chemical challenges in the creation of artificial viruses,” *Chem. Rev. Soc.* **41**, 2562 (2012).
- [12] U. Lächelt and E. Wagner, “Nucleic acid therapeutics using polyplexes: A journey of 50 years (and beyond).” *Chem. Rev.* **115**, 11043 (2015).
- [13] Z. Ou and M. Muthukumar, “Entropy and enthalpy of polyelectrolyte complexation: Langevin dynamics simulations,” *J. Chem. Phys.* **124**, 154902 (2006).
- [14] S. Liu and M. Muthukumar, “Langevin dynamics simulation of counterion distribution around isolated flexible polyelectrolyte chains,” *J. Chem. Phys.* **116**, 9975 (2002).
- [15] S. Liu, K. Ghosh, and M. Muthukumar, “Polyelectrolyte solutions with added salt: A simulation study,” *J. Chem. Phys.* **119**, 1813 (2003).
- [16] Z. Ou and M. Muthukumar, “Langevin dynamics of semiflexible polyelectrolytes: Rod-toroid-globule-coil structures and counterion distribution,” *J. Chem. Phys.* **123**, 074905 (2005).
- [17] P.-Y. Hsiao and E. Luijten, “Salt-induced collapse and reexpansion of highly charged flexible polyelectrolytes,” *Phys. Rev. Lett.* **97**, 148301 (2006).
- [18] P.-Y. Hsiao, “Chain morphology, swelling exponent, persistence length, like-charge attraction, and charge distribution around a chain in polyelectrolyte solutions: effects of salt concentration and ion size studied by molecular dynamics simulations,” *Macromolecules* **39**, 7125 (2006).
- [19] P.-Y. Hsiao, “Linear polyelectrolytes in tetravalent salt solutions,” *J. Chem. Phys.* **124**, 044904 (2006).
- [20] D. Srivastava and M. Muthukumar, “Interpenetration of interacting polyelectrolytes,” *Macromolecules* **27**, 1461 (1994).

- [21] R. G. Winkler, M. O. Steinhauser, and P. Reineker, "Complex formation in systems of oppositely charged polyelectrolytes: A molecular dynamics simulation study," *Phys. Rev. E* **66**, 021802 (2002).
- [22] Y. Hayashi, M. Ullner, and P. Linse, "A Monte Carlo study of solutions of oppositely charged polyelectrolytes," *J. Chem. Phys.* **116**, 6836 (2002).
- [23] Y. Hayashi, M. Ullner, and P. Linse, "Complex formation in solutions of oppositely charged polyelectrolytes at different polyion compositions and salt content," *J. Phys. Chem. B* **107**, 8198 (2003).
- [24] Y. Hayashi, M. Ullner, and P. Linse, "Oppositely charged polyelectrolytes. complex formation and effects of chain asymmetry," *J. Phys. Chem. B* **108**, 15266 (2004).
- [25] R. S. Dias, A. A. C. C. Pais, M. G. Miguel, and B. Lindman, "Modeling of DNA compaction by polycations," *J. Chem. Phys.* **119**, 8150 (2003).
- [26] M. J. Stevens and K. Kremer, "The nature of flexible linear polyelectrolytes in salt free solution: A molecular dynamics study," *J. Chem. Phys.* **103**, 1669 (1995).
- [27] J. D. Weeks, D. Chandler, and H. C. Andersen, "Role of repulsive forces in determining the equilibrium structure of simple liquids," *J. Chem. Phys.* **54**, 5237 (1971).
- [28] R.W. Hockney and J.W. Eastwood, *Computer Simulation Using Particles* (Adam Hilger, Bristol, 1988).
- [29] M. Deserno and C. Holm, "How to mesh up Ewald sums. I. A theoretical and numerical comparison of various particle mesh routines," *J. Chem. Phys.* **109**, 7678–7693 (1998).
- [30] W. C. Swope, H. C. Andersen, P. H. Berens, and K. R. Wilson, "A computer simulation method for the calculation of equilibrium constants for the formation of physical clusters of molecules: Application to small water clusters," *J. Chem. Phys.* **76**, 637 (1982).
- [31] D. Frenkel and B. Smit, *Understanding Molecular Simulation*, 2nd ed. (Academic Press, 2002).
- [32] H.J. Limbach, A. Arnold, B.A. Mann, and C. Holm, "ESPResSo—an extensible simulation package for research on soft matter systems," *Comput. Phys. Commun.* **174**, 704 (2006).
- [33] W. Humphrey, A. Dalke, and K. Schulten, "VMD – visual molecular dynamics," *Journal of Molecular Graphics* **14**, 33 (1996).
- [34] M. O. de la Cruz, L. Belloni, M. Delsanti, J. P. Dalbiez, O. Spalla, and M. Drifford, "Precipitation of highly charged polyelectrolyte solutions in the presence of multivalent salts," *J. Chem. Phys.* **103**, 5781 (1995).
- [35] D. Mukherji, C. M. Marques, and K. Kremer, "Polymer collapse in miscible good solvents is a generic phenomenon driven by preferential adsorption," *Nat. Commun.* **5**, 4882 (2014).
- [36] B. Peng and M. Muthukumar, "Modeling competitive substitution in a polyelectrolyte complex," *J. Chem. Phys.* **143**, 243133 (2015).
- [37] Q. Leng, M. C. Woodle, P. Y. Lu, and A. J. Mixson, "Advances in systemic siRNA delivery," *Drugs Fut.* **34**, 721 (2009).
- [38] K. A. Whitehead, R. Langer, and D. G. Anderson, "Knocking down barriers: advances in siRNA delivery," *Nat. Rev. Drug Discovery* **8**, 129 (2009).
- [39] M. E. Davis, J. E. Zuckerman, C. H. J. Choi, D. Seligson, A. Tolcher, C. A. Alabi, Y. Yen, J. D. Heidel, and A. Ribas, "Evidence of RNAi in humans from systemically administered siRNA via targeted nanoparticles," *Nature* **464**, 1067 (2010).